

Synthesis, antiproliferative, antioxidant activities, *in silico* studies, DFT analysis and molecular dynamics simulation of novel 1-(4-chlorobenzhydryl) piperazine derivatives

Najim A. Al-Masoudi^{a,1,*}, Raad S. Jihad^b, Nabeel A. Abdul-Rida^c, Amer M.J. Al-Shamari^d, Bahjat A. Saeed^e, Wasfi A. Al-Masoudi^f, Amneh Shtaiwi^g, Yaseen A. Al-Soud^h

^a Department of Chemistry, College of Science, University of Basrah, Basrah, Iraq

^b General Directorate of Muthana Education, Muthana, Iraq

^c Department of Chemistry, University of Al-Qadisiya, Al-Qadisiya, Iraq

^d Department of Chemistry, College of Science, University of Kufa, Kufa, Iraq

^e Department of Chemistry, College of Education for Pure Science, University of Basrah, Basrah, 61001, Iraq

^f Department of Physiology, Pharmacology and Chemistry, College of Veterinary, University of Basrah, Basrah, 61001, Iraq

^g Faculty of Pharmacy, Middle East University, Queen Alia Airport Street, Amman, 11610, Jordan

^h Department of Chemistry, College of Science, University of Al al-Bayt, Al-Mafraq, Jordan

ARTICLE INFO

Keywords:

Anticancer activity
Antioxidant activity
Benzhydryl piperazine
Docking study
Molecular dynamics simulation
DTF analysis

ABSTRACT

A series of 1-(4-chlorobenzhydryl) piperazine derivatives **3–10** were synthesized and characterized both spectroscopically and structurally to investigate their antiproliferative activity associated with the piperazine framework. The compounds were screened against seven human cell lines. Analogously, compounds **14–16** were prepared from treatment of **2** with 4-((2-aminothiazol-4-yl)amino)phenol (**11**), 4-((2-aminothiazol-4-yl)phenol (**12**) or 2-amino-5-methoxybenzothiazole (**13**) in the presence of K₂CO₃ and KI. Compounds **7** and **10** displayed the highest potency, where **7** exhibited an IC₅₀ value of 6.85 μM against the Z-138-non Hodgkin lymphoma cancer cell line, and **10** showed IC₅₀ of 7.40 μM against the DND-41 acute lymphoblastic leukemia cancer cell line. However, all compounds demonstrated IC₅₀ values ranging from 22.0 to > 100 μM against other tested cancer cell lines. These findings suggest that compounds **7** and **10** hold promise as potential lead compounds for the development of novel antiproliferative agents. Furthermore, compounds **3–10**, and **14–16** were evaluated for their antioxidant activity. The study encompassed the molecular docking analysis of compound **7** alongside specific amino acids present in Z-138-non-Hodgkin lymphoma (phosphoinositide 3-kinase, protein PI3kδ, PDB: 4XE0), as well as the docking assessment of compound **10** with the amino acids present in DND-41-acute lymphoblastic leukemia (receptor tyrosine phosphatase (PTPRC/CD45, PDB: 1YGR). The molecular dynamics simulation as well as the DFT have been performed.

1. Introduction

Benzhydryl piperazine derivatives have received significant attention due to their diverse biological activities, such as antifungal and antibacterial [1–4], anticancer agents [5–7], and antihistaminic [8–11] agents. Additionally, these compounds display a diverse array of pharmacological activities, including antiviral effects [12,13], calcium channel blocking capabilities [14–19], and acting as selective dopamine D3 receptor ligands [20]. These biological activities are a driving force for the synthetic

chemists to focus on this important class of condensed benzhydryl piperazine scaffold with aliphatic or aromatic precursors. However, drugs having benzhydryl piperazines such as cetirizine, cinnarizine, clocinnazine, cyclizine, meclizine, hydroxyzine, and dotarizine can act as antihistamine compounds and calcium channel blockers as well as antagonists at the 5HT_{2A} receptor. On the other hand, some of benzhydryl piperazine derivatives exhibited potential activity as anticancer agents. Kumar et al. [21] has reported the cytotoxicity of several 1-benzhydryl piperazine derivatives substituted with variable sulfonyl chlorides, acid chlorides,

* Corresponding author.

E-mail address: najim.al-masoudi@gmx.de (N.A. Al-Masoudi).

¹ Present address: Department of Chemistry, College of Science, University of Basrah, 78464 Konstanz, Germany

and isothiocyanates. These analogues exhibited potent cytotoxicity against breast cancer (MCF-7), hepatocellular carcinoma (HepG-2), cervix carcinoma (HeLa) and colon carcinoma (HT-29) cell lines. Yarim et al. [22] has described the synthesis of 1-(4-substituted-benzoyl)-4-(4-chloro-benzhydryl)piperazine derivatives and their effect on the inhibition of cancer cell lines from liver, breast, colon, gastric, and endometrial samples. A series of 1-benzhydryl-sulfonyl-piperazine derivatives have been synthesized and evaluated for their efficacy in inhibiting MDA-MB-231 breast cancer cell proliferation, where compound 1-benzhydryl-4-(4-*tert*-butyl-benzenesulfonyl)-piperazine showed significant inhibitory activity [23]. In a study conducted by Gan et al. [24], certain benzhydryl derivatives containing imidazole and 1,2,3-triazole moieties showed promising activity against the human prostatic carcinoma (PC-3) cell line. Similarly, Gurdal et al. [25] investigated the cytotoxicity of derivatives of 1-(substituted-benzoyl)-4-benzhydryl piperazine and 1-[(substituted-phenyl) sulfonyl]-4-benzhydryl piperazine. Additionally, Razic et al. [26] recently reported the synthesis of new 1-benzhydryl piperazine-based isoform-selective histone deacetylase (HDAC) inhibitors. One of these analogues, featuring phenylhydroxamic acid, demonstrated selective HDAC6 inhibition with an IC₅₀ value of 30 nM. Furthermore, da Silva et al. [27] have reported the in vitro hepatotoxicity of 'Legal X': the combination of 1-benzylpiperazine (BZP) and 1-(*m*-trifluoromethylphenyl)piperazine (TFMPP) triggers oxidative stress, mitochondrial impairment and apoptosis, meanwhile Valkova et al. [28] described the synthesis of novel 1-arylpiperazine derivatives and assessed their affinity for 5-HT1A/5-HT2A receptors, noting that one of the analogues exhibited a high affinity value. In addition, Murthy et al. [29] identified certain benzhydryl piperazine-coupled nitrobenzenesulfonamide hybrids as active compounds against the *Mycobacterium tuberculosis* H37Rv strain, displaying low cytotoxicity with a selectivity index (SI) greater than 30. A review concerning the synthesis of the biomedical synthesis and the biochemical application of benzhydryl amines in the pharmaceutical area from 2015 to 2019 has been reported by Roy and Panda [30], whereas Shtaiwi et al. [31] investigated the binding mechanism of the newly designed benzophenone imine inhibitors with the human estrogen receptor to treat the breast cancer.

In view of such biological properties of benzhydryl piperazine derivatives and as our earlier study to develop new anticancer agents [32–39], we report herein the synthesis of novel benzhydryl piperazine derivatives incorporating sulfa drugs and thiazole derivatives with evaluation of their antiproliferative and antioxidant activities, alongside a comprehensive study involving molecular docking, density functional theory (DFT) analysis, and molecular dynamics simulation.

2. Experimental section

2.1. General information

Melting points were determined on a Mel-Temp device melting point apparatus and are uncorrected. The IR spectra were recorded, on FT-IR Spectrophotometer (Thermo Nicolet Corp. USA), using KBr discs. ¹H and ¹³C NMR spectra were recorded on Bruker Avance (400 MHz) (¹H) and 100 MHz (¹³C) spectrometers, using DMSO-d₆ solvent containing tetramethylsilane as an internal standard (chemical shifts in δ in ppm). The reactions were monitored by thin layer chromatography, (eluent: hexane-EtOAc 4:1), and the spots were visualized by iodine and U.V. Microwave supported reactions were performed with microwave cavity at 2.4 GHz, temperature from 0 to 300 °C in microwave reaction vials (2.5 mL) with Teflon septum and an aluminum crimp top.

2.2. 2-Chloro-1-(4-((4-chlorophenyl)phenylmethyl)piperazin-1-yl)ethan-1-one (2)

To a solution of 1-(4-chlorobenzhydryl)piperazine (1) (500 mg, 1.75 mmol) and triethylamine (0.20 mL) in dry CH₂Cl₂ (20 mL) at 0 °C was added 2-chloro-acetyl chloride (0.11 mL, 2.62 mmol) dropwise. The

reaction mixture was stirred at 0 °C for 2 h and the stirring was continued at room temperature for another 2 h. The reaction was quenched with distilled water and extracted with CHCl₃ (3 × 30 mL). The organic layer was washed with 10 % NH₄Cl solution and then water and dried (MgSO₄). The crude product was purified on SiO₂ column (20 g) using toluene-ethyl acetate (6:1) as eluent to give 2 (432 mg, 68 %) as light brown solid; mp: 88–90 °C; R_f = 0.55; FT-IR (KBr, cm⁻¹): ν_{max} 2980, 2939 (C–H), 1590 (C=C), 1661 (C=O), 3050 (C–H); ¹H NMR (400 MHz, DMSO-d₆): δ 2.67, 3.64 (m, 8H, H_{piperazine}), 4.35 (s, 2H, CH₂Cl), 4.89 (s, 1H, CH_{bridge}), 7.24–7.77 (m, 9H, H_{arom.}); ¹³C NMR (100 MHz, DMSO-d₆): δ 41.4 (CH₂Cl), 42.2, 51.3, 51.6 (C_{piperazine}), 74.0 (C_{bridge}), 126.4 128.3, 129.2, 129.3, 130.1 132.0, 141.3 (C_{arom.}), 165.0 (C=O). Elemental analysis calcd for C₁₉H₂₀C₁₂N₂O (363.28): C, 62.82; H, 5.55; N, 7.71. Found: C, 62.74; H, 5.48; N, 7.63.

2.3. General procedure for the synthesis of 4-((2-(4-((4-chlorophenyl)phenylmethyl)piperazin-1-yl)-2-oxoethyl)amino)-N-(aryl)benzenesulfonamide (3–10)

A solution of 4-amino-N-aryl-benzenesulfonamide (0.6 mmol) in EtOH (5 mL) was added to a stirred solution of 2 (182 mg, 0.50 mmol) in dry EtOH (10 mL), followed by the addition of K₂CO₃ (102 mg, 0.74 mmol) and a catalytic amount of KI (5.0 mg, 0.03 mmol). The heated under reflux for 8 h. After cooling, the mixture was filtered and filtrate was evaporated to dryness under reduced pressure. The residue was partitioned between CH₂Cl₂ (3 × 15 mL) and water (15 mL). The combined organic layers were dried (Na₂SO₄), filtered and the filtrate was evaporated to dryness. The residue was purified on a short column of silica gel using hexane-EtOAc (3:2) as eluent to give the pure desired product.

2.3.1. 4-((2-(4-((4-Chlorophenyl)phenylmethyl)piperazin-1-yl)-2-oxoethyl)amino)-N-(pyridin-2-yl)benzenesulfonamide (3)

From sulfapyridine (149 mg). Yield: (235 mg, 83 %) as yellow solid; mp: 144–146 °C; R_f = 0.66; FT-IR (KBr, cm⁻¹): ν_{max} 2936, 2850 (C–H), 3389, 3226 (N–H), 3061 (C–H_{arom.}), 1632 (C=O), 1596, 1501 (C=C_{arom.}) 1330 (SO₂); ¹H NMR (400 MHz, DMSO-d₆): δ 2.73, 3.44, 3.46 (m, 8H, H_{piperazine}), 3.86 (s, 2H, CH₂), 4.84 (s, 1H, CH_{bridge}), 6.56 (m, 1H, H_{pyridine-3'}), 6.70 (m, 1H, H_{pyridine-5'}), 7.07–7.67 (m, 14H, H_{arom.}) 8.10 (dd, 1H, J = 7.9, 3.5 Hz, H_{pyridine-6'}), 10.30 (br, 1H, NH); ¹³C NMR (100 MHz, DMSO-d₆): δ 44.4, 51.4 (C_{piperazine}), 56.5 (CH₂), 74.0 (C_{bridge}), 111.5 (C_{pyridine-3'}), 117.5 (C_{pyridine-5'+C_{arom.}}), 126.2, 128.1, 130.0, 130.2 131.9, 139.2, 141.8, 142.5 (C_{arom.}), 152.0 (C_{pyridine-6'}), 153.2 (C_{pyridine-2'}), 172.3 (C=O). Elemental analysis calcd for C₃₀H₃₀ClN₅O₃S (576.11): C, 62.55; H, 5.25; N, 12.16. Found: C, 62.48; H, 5.17; N, 12.09.

2.3.2. 4-((2-(4-((4-Chlorophenyl)phenylmethyl)piperazin-1-yl)-2-oxoethyl)amino)-N-(pyrimidin-2-yl)benzenesulfonamide (4)

From the sulfadiazine (150 mg). Yield: 233 mg, (81 %) as yellow solid; mp: 159–161 °C; R_f = 0.82; FT-IR (KBr, cm⁻¹): ν_{max} 3258, 3355 (NH), 3070, 2962, 2811 (C–H), 1652 (C=O), 1581 (C=C_{arom.}), 1324 (SO₂); ¹H NMR (400 MHz, DMSO-d₆): δ 2.94, 3.49 (m, 8H, H_{piperazine}), 3.59 (s, 2H, CH₂), 5.73 (s, 1H, CH_{bridge}), 6.09 (br., 1H, NH), 7.02 (m, 1H, H_{pyrimidine-5'}), 7.27–7.57 (m, 13H, H_{arom.}), 8.34 (m., 2H, H_{pyrimidine-4'+H_{pyrimidine-6'}}), 11.34 (br, 1H, NH); ¹³C NMR (100 MHz, DMSO-d₆): δ 47.0, 51.4, (C_{piperazine}), 56.5 (CH₂), 74.0 (C_{bridge}), 112.6, 116.0, 125.3, 127.7, 128.1, 128.3, 129.0, 129.3, 129.7, 129.9, 130.3, 132.0, 139.3, 142.0 (C_{arom.}+C_{pyrimidine-5'}), 157.7 (C_{pyrimidine-4'+C_{pyrimidine-6'}}), 170.3 (C = O+C_{pyrimidine-2'}). Elemental analysis calcd for C₂₉H₂₉ClN₅O₃S (577.10): C, 60.36; H, 5.07; N, 14.56. Found: C, 60.30; H, 5.01; N, 14.50.

2.3.3. 4-((2-(4-((4-Chlorophenyl)phenylmethyl)piperazin-1-yl)-2-oxoethyl)amino)-N-(4,6-dimethyl pyrimidin-2-yl)benzenesulfonamide (5)

From sulfamethazine (167 mg). Yield: 254 mg (84 %) as yellow brown solid; mp: 155–157 °C; R_f = 0.74; FT-IR (KBr, cm⁻¹): ν_{max} 3050,

2962, 2813 (C—H), 1755 (C=N), 1655 C=O, 1597, 1542, 1487 (C=C_{arom.}), 1330 (SO₂); ¹H NMR (400 MHz, DMSO-*d*₆): δ 2.33 (s, 6H, 2xMe), 2.93, 2.99, 3.53 (m, 8H, H_{piperazine}), 3.56 (s, 1H, CH₂), 4.89 (s, 1H, CH_{bridge}), 6.71 (s, 1H, NH), 7.07 (s, 1H, H_{pyrimidine-5'}), 7.26–7.85 (m, 13H, H_{arom.}), 11.37 (br., 1H, NH); ¹³C NMR (100 MHz, DMSO-*d*₆): δ 24.6 (2xMe), 45.9, 51.8 (C_{piperazine}), 56.5 (CH₂), 74.1 (C_{bridge}), 109.4 (C_{pyrimidine-3'}), 111.5, 126.2, 127.9, 128.2, 129.2, 129.4, 130.0, 131.0, 132.0, 142.3, 144.7 (C_{arom.}), 164.6 (C_{pyrimidine-4'}), 165.6 (C_{pyrimidine-2'}), 170.4 (C=O+C_{pyrimidine-6'}). Elemental analysis calcd for C₃₁H₃₃ClN₆O₃S (605.15): C, 61.53; H, 5.50; N, 13.89. Found: C, 61.47; H, 5.43; N, 13.84.

2.3.4. 4-((2-(4-((4-Chlorophenyl)phenylmethyl)piperazin-1-yl)-2-oxoethyl)amino)-N-(5-methyl-isoxazol-3-yl)benzenesulfonamide (6)

From sulfamethoxazole (152 mg). Yield: 232 mg (80 %) as yellow-brown solid; mp: 120–122 °C; R_f = 0.78; FT-IR (KBr, cm⁻¹): ν_{max} 3221, 3351 (N—H), 3058, 3026, 2962, 2925, 2813 (C—H), 1660 (C=O), 1595, 1488 C=C; ¹H NMR (400 MHz, DMSO-*d*₆): δ 2.31 (s, 1H, Me), 2.99, 3.40 (m, 8H, H_{piperazine}), 3.56 (s, 2H, CH₂), 5.36 (s, 1H, CH_{bridge}), 6.32 (s, 1H, H_{methoxazole-4'}), 6.72 (br s., 1H, NH), 6.99–7.71 (m, 13H, H_{arom.}), 10.52 (br s., 1H, NH); ¹³C NMR (100 MHz, DMSO-*d*₆): δ 12.6 (Me), 46.1, 51.8 (C_{piperazine}), 54.2 (CH₂), 74.1 (C_{bridge}), 95.8 (C_{methoxazole-4'}), 113.1, 123.0, 127.6, 128.1, 128.3, 129.0, 129.2, 129.9, 131.9, 142.0, 142.4 (C_{arom.}), 151.4 (C_{methoxazole-5'}), 164.9 (C=O), 170.5 (C_{methoxazole-3'}). Elemental analysis calcd for C₂₉H₃₀ClN₅O₄S (580.10): C, 60.04; H, 5.21; N, 12.07; S, 5.53. Found: C, 59.93; H, 5.12; N, 11.99.

2.3.5. 4-((2-(4-((4-Chlorophenyl)phenylmethyl)piperazin-1-yl)-2-oxoethyl)amino)-N-(thiazol-2-yl)benzenesulfonamide (7)

From sulfathiazole (153 mg). Yield: 21 mg (83 %) as yellow solid; mp: 132–135 °C; R_f = 0.81; FT-IR (KBr, cm⁻¹): ν_{max} 3390 (N—H), 3058, 3026, 2926, 2811 (C—H), 1653 (C=O), 1597, 1509 (C=C), 1330(SO₂); ¹H NMR (400 MHz, DMSO-*d*₆): δ 2.94, 3.47 (m, 8H, H_{piperazine}), 3.79 (s, 2H, CH₂), 4.86 (s, 1H, H_{bridge}), 6.80 (br s., 1H, H_{thiazole-5'}), 7.19–7.77 (m, 14H, H_{arom.}+H_{thiazole-4'}), 12.52 (br s., 1H, NH); ¹³C NMR (100 MHz, DMSO-*d*₆): δ 44.4, 51.3 (C_{piperazine}), 56.5 (CH₂), 74.0 (C_{bridge}), 112.9 (C_{thiazole-5'}), 124.7, 127.9, 128.2, 128.3, 129.1, 129.2, 130.1, 132.0, 136.8, 141.8, 142.3 (C_{arom.}+C_{thiazole-4'}), 171.0 (C=O), 173.6 (C_{thiazole-2'}). Elemental analysis calcd for C₂₈H₂₈ClN₅O₃S₂ (582.13): C, 57.77; H, 4.85; N, 12.03. Found: C, 57.71; H, 6.01; N, 11.96.

2.3.6. 4-((2-(4-((4-Chlorophenyl)phenylmethyl)piperazin-1-yl)-2-oxoethyl)amino)benzenesulfonic acid (8)

From sulfanilic acid (179 mg). Yield: 206 mg (81 %) as brown solid; mp: 150–152 °C; R_f = 0.74; FT-IR (KBr, cm⁻¹): ν_{max} 3419 (O—H and N—H), 3058, 3027, 2963, 2916, 2857, 2813 (C—H), 1648 (C=O), 1602 (C=C), 1336 (SO₂); ¹H NMR (400 MHz, DMSO-*d*₆): δ 3.40, 3.51, 3.53 (m, 8H, H_{piperazine}), 3.92 (s, 2H, CH₂), 5.22 (s, 1H, CH_{bridge}), 6.57 (s, 1, NH), 7.24–7.82 (m, 17H, H_{arom.}), 8.34 (s, 1H, OH); ¹³C NMR (100 MHz, DMSO-*d*₆): δ 56.5 (CH₂), 44.0, 51.5 (C_{piperazine}), 74.1 (C_{bridge}), 112.7 (C_{sulfonic acid-2'}+C_{sulfonic acid-6'}), 124.7, 127.9, 128.2, 128.3, 129.1, 129.2, 129.4, 130.0, 132.0, 136.8, 141.7, 142.3 (C_{arom.}), 170.4 (C=O)). Elemental analysis calcd for C₂₅H₂₆ClN₅O₄S (500.01): C, 60.05; H, 5.24; N, 8.40. Found: C, 60.00; H, 5.24; N, 8.34.

2.3.7. 4-((2-(4-((4-Chlorophenyl)phenylmethyl)piperazin-1-yl)-2-oxoethyl)amino)benzene sulfonamide (9)

From sulfanilamide (196 mg). Yield: 197 mg (79 %) as brown solid; mp: 96–98 °C; R_f = 0.88; FT-IR (KBr, cm⁻¹): ν_{max} 3426 (N—H), 3024, 2966, 2854 (C—H), 1652 (C=O), 1596 (C=C), 1335 (SO₂); ¹H NMR (400 MHz, DMSO-*d*₆): δ 3.05, 3.07, 3.52 (m, 8H, H_{piperazine}), 3.88 (s, 2H, CH₂), 4.84 (s, 1H, CH_{bridge}), 6.36 (br., 1H, NH₂), 7.05–7.77 (m, 13H, H_{arom.}), 9.90 (br., 1H, NH); ¹³C NMR (100 MHz, DMSO-*d*₆): δ 46.0, 51.8 (C_{piperazine}), 54.2 (CH₂), 74.1 (C_{bridge}), 112.9 (C_{sulfonamide-2'}+C_{sulfonamide-6'}), 127.0, 127.7, 128.1, 129.0, 129.2, 129.9, 131.9, 137.1, 141.9, 142.3 (C_{arom.}), 172.5 (C=O). Elemental analysis calcd for C₂₅H₂₇ClN₄O₃S (499.03): C, 60.17; H, 5.45; N, 11.23. Found: C, 60.01; H, 5.29; N, 11.08.

2.3.8. 2,2'-((Sulfonyl-bis(4,1-phenylene))bis(azanediyl))bis(1-(4-((4-chlorophenyl)phenylmethyl)piperazin-1-yl)ethan-1-one) (10)

From dapsone (149 mg). Yield: 383 mg (85 %), as yellow solid; mp: 129–132 °C; R_f = 0.63; FT-IR (KBr, cm⁻¹): ν_{max} 3243 (N—H), 3040, 3070, 2962, 2923, 2812, (C—H), 1651(C=O), 1596 (C=C), 1317 (SO₂); ¹H NMR (400 MHz, DMSO-*d*₆): δ 2.94, 3.86 (m, 8H, H_{piperazine}), 3.43 (s, 2H, CH₂), 5.06 (s, 1H, CH_{bridge}), 6.32 (s, 1H, NH), 6.66–7.87 (m, 26H, H_{arom.}); ¹³C NMR (100 MHz, DMSO-*d*₆): δ 54.2 (CH₂), 45.1, 51.8 (C_{piperazine}), 73.9 (C_{bridge}), 112.91, 126.4, 127.9, 128.1, 129.0, 129.2, 129.3, 129.9, 129.9, 132.0, 141.7, 142.1 (C_{arom.}), 173.3 (C=O). Elemental analysis calcd for C₅₀H₅₀C₁₂N₆O₄S (901.95): C, 66.58; H, 5.59; N, 9.32. Found: C, 66.46; H, 5.47; N, 9.21.

2.4. General procedure for the synthesis of 1-(4-chlorobenzhydryl)piperazine conjugated 2-aminothiazole derivatives (14–16)

To a suspension of 2 (300 mg, 0.83 mmol) and K₂CO₃ (171 mg, 1.24 mmol) in EtOH (20 mL), 2-aminothiazole derivatives (0.83 mmol) and a catalytic amount of KI (8 mg, 0.049 mmol) were added. The resulting mixture was stirred at 20 °C for 2 h (followed by TLC). The suspension was filtered, and the filtrate was evaporated to dryness. The residue was suspended in water (10 mL) and extracted with CH₂Cl₂ (3 × 30 mL). The combined organic layers were dried (Na₂SO₄), filtered and evaporated to dryness. The crude product was purified on a short column of SiO₂ (5 g) using hexane-EtOAc (3:2) as eluent to give the desired pure product.

2.4.1. 1-(4-((4-Chlorophenyl)phenylmethyl)piperazin-1-yl)-2-((4-((4-hydroxyphenyl)amino)thiazol-2-yl)amino)ethan-1-one (14)

From 4-((2-aminothiazol-4-yl)amino)phenol (11) (172 mg). Yield: 346 mg (78 %) as brown solid; mp: 92–94 °C; R_f = 0.89; FT-IR (KBr, cm⁻¹): ν_{max} 3340, 3249 (N—H + OH), 3059, 2973, 2936, 2801 (C—H), 1646 (C=O), 1513, 1473 (C=C); ¹H NMR (400 MHz, DMSO-*d*₆): δ 2.94, 3.86 (m, 8H, H_{piperazine}), 3.90 (s, 2H, CH₂), 5.45 (s, 1H, CH_{bridge}), 5.72 (s, 1H, H_{thiazole-5'}), 6.15 (s, 1H, NH), 7.02–7.47 (m, 13H, H_{arom.}), 8.83 (s, 1H, NH), 9.27 (br s., 1H, OH); ¹³C NMR (100 MHz, DMSO-*d*₆): δ 45.1, 51.8 (C_{piperazine}), 60.4 (CH₂), 74.1 (C_{bridge}), 104.1 (C_{thiazole-5'}), 115.5, 116.6, 121.2, 127.7, 128.0, 128.1, 129.0, 129.1, 129.9, 131.7, 133.0, 139.9, 142.1 (C_{arom.}), 149.0 (C—OH), 153.4 (C_{thiazole-4'}), 162.5 (C_{thiazole-2'}), 172.5 (C=O). Elemental analysis calcd for C₂₈H₂₈ClN₅O₂S (534.08): C, 62.97; H, 5.28; N, 13.11. Found: C, 62.86; H, 5.16; N, 13.00.

2.4.2. 1-(4-((4-Chlorophenyl)phenylmethyl)piperazin-1-yl)-2-((4-((4-hydroxyphenyl)thiazol-2-yl)amino)ethan-1-one) (15)

From 4-((2-aminothiazol-4-yl)phenol) (12) (mg). Yield: mg (74 %); as brown solid; mp: 74–76 °C; R_f = 0.87; FT-IR (KBr, cm⁻¹): ν_{max} 3390 (OH), 3197 (NH), 3050, 2974, 2938, 2854 (C—H), 1619 (C=O), 1514, 1472 (C=C); ¹H NMR (400 MHz, DMSO-*d*₆): δ 2.95, 3.41 (m, 8H, H_{piperazine}), 3.57 (s, 2H, CH₂), 5.72 (s, 1H, CH_{bridge}), 6.15 (s, 1H, NH), 7.09 (s, 1H, H_{thiazole-5'}), 7.15–7.86 (m, 13H, H_{arom.}), 6.87 (s, 1H, NH), 9.80 (s., 1H, OH); ¹³C NMR (100 MHz, DMSO-*d*₆): δ 45.8, 51.6 (C_{piperazine}), 60.5 (CH₂), 73.9 (C_{bridge}), 110.7 (C_{thiazole-5'}), 115.9, 124.0, 126.1, 128.7, 129.6, 129.8, 131.1, 141.1 (C_{arom.}), 153.1 (C_{thiazole-4'}), 158.1 (C—OH), 166.9 (C_{thiazole-2'}), 169.4 (C=O). Elemental analysis calcd for C₂₈H₂₇ClN₄O₂S (519.06): C, 64.79; H, 5.24; N, 10.79. Found: C, 64.72; H, 5.16; N, 10.71.

2.4.3. 1-(4-((4-Chlorophenyl)phenylmethyl)piperazin-1-yl)-2-((5-methoxyvenzo[d]thiazol-2-yl)amino)ethan-1-one (16)

From 2-amino-5-methoxybenzothiazole (13) (mg). Yield: mg (79 %); as brown solid; mp: 135–137 °C; R_f = 0.67; FT-IR (KBr, cm⁻¹): ν_{max} 3297 (NH), 3050, 2963, 2902, 2830 (C—H), 1652 (C=O), 1575, 1543, 1468 (C=C); ¹H NMR (400 MHz, DMSO-*d*₆): δ 2.94, 3.44 (m, 8H, H_{piperazine}), 3.57 (s, 2H, CH₂), 3.79 (s, 3H, OMe), 5.38 (s, 1H, CH_{bridge}), 6.80 (s, 1H, NH), 7.07–7.52 (m, 12H, H_{arom.}); ¹³C NMR (100 MHz, DMSO-*d*₆): δ 47.3, 51.2 (C_{piperazine}), 56.5 (OMe), 60.4 (CH₂), 73.9 (C_{bridge}), 106.0

(C_{benzothiazole-4}), 113.3 (C_{benzothiazole-6}), 118.5 (C_{benzothiazole-7a}), 127.7, 128.1, 129.1, 129.2, 129.9, 132.0, 141.8, 142.2, 142.3 (C_{arom.}), 147.3 (C_{benzothiazole-3a}), 154.8 (C_{benzothiazole-5}), 168.3 (C=O), 170.4 (C_{benzothiazole-2}). Elemental analysis calcd for C₂₇H₂₇ClN₄O₂S (507.05): C, 63.96; H, 5.37; N, 11.05. Found: C, 63.90; H, 5.31; N, 11.00.

2.5. Biological assays

2.5.1. In vitro anticancer activity

2.5.1.1. Cancer cell lines. The human cancer cell lines utilized in this manuscript, including Capan-1, HCT-116, LN-229, NCI-H460, HL-60, K-562, H, and Z-138 cancer cells, were obtained from the American Type Culture Collection (ATCC, Manassas, VA, USA). The DND-41 cell line was acquired from the Deutsche Sammlung von Mikroorganismen und Zellkulturen (DSMZ Leibniz-Institut, Germany). Culture media were procured from Gibco Life Technologies, USA, and supplemented with 10 % fetal bovine serum (HyClone, GE Healthcare Life Sciences, USA), except for the media for other cell lines, which were purchased from Sigma.

2.5.1.2. Proliferation assays. The adherent cell lines LN-229, HCT-116, NCI-H460, and Capan-1 cells were plated in 384-well tissue culture plates (Greiner) at a density ranging from 500 to 1500 cells per well. Following an overnight incubation, the cells were exposed to seven different concentrations of the test compounds, ranging from 100 to 0.006 μ M. For the suspension cell lines HL-60, K-562, Z-138, and DND-41, densities ranging from 2500 to 5500 cells per well were used in 384-well culture plates containing the same concentration points of the test compounds. The cells were then incubated with the compounds for 72 h and subjected to analysis using the CellTiter 96[®] Aqueous One Solution Cell Proliferation Assay (MTS) reagent (Promega), following the manufacturer's instructions. Absorbance measurements were taken at 490 nm using a SpectraMax Plus 384 (Molecular Devices), and the optical density (OD) values were utilized to determine the 50 % inhibitory concentration (IC₅₀). Two independent experiments were conducted for compound testing. HeLa cells were seeded in 96-well microtiter plates at a concentration ranging from 1×10^4 to 3×10^4 cells/mL, depending on the doubling times of the specific cell line. Test agents were added in five 10-fold dilutions (10^{-8} to 10^{-4} M). Fresh working dilutions were prepared on the day of testing. After 72 h of incubation, the cell growth rate was assessed using the MTS assay, following the previously described method [40]. Absorbance measurements were taken at 570 nm, and the OD values were used to calculate the 50 % inhibitory concentration (IC₅₀). Each test was performed in duplicate in at least two separate experiments.

2.5.2. Antioxidant assay by using DPPH radical scavenging method

The DPPH (1,1-diphenyl-2-picrylhydrazyl) free radical scavenging assay was employed to evaluate the antioxidant activity of the synthesized compounds **3–10**. Initially, a 0.2 mM solution of DPPH in ethanol was prepared. Then, 1.0 mL of this solution was added to 3.0 mL of compound solution in ethanol at various concentrations (1000, 900, 800, 700, 600, 500, 250, 125, 62.5, 31.25 μ g/mL). The mixture was vigorously shaken and left to stand at room temperature for 30 min. Subsequently, the absorbance was measured at 517 nm using a UV–VIS spectrophotometer (UV–VIS Shimadzu). The antioxidant activity of the tested compounds was determined by calculating the percentage of DPPH neutralization and comparing it to the standard antioxidant, ascorbic acid. The percent DPPH scavenging effect was calculated using the following equation:

$$DPPH\text{scavengingeffect(\%)}\text{or\%inhibition} = (Ac(0) - AA(t))/Ac(0) \times 100$$

where Ac(0) represents the absorbance of the control at $t = 0$, and AA(t) is the absorbance of the antioxidant at $t = 30$ min. All measurements

were performed in triplicate

2.6. In silico studies

2.6.1. Molecular docking

Molecular docking of the compounds **7** and **10** with phosphoinositide 3-kinases (PI3k δ), pdb: 4xe0, and tyrosine phosphatase PTPRC (CD45) pdb: 1ygr, were performed using Glide available in Maestro 13.0. Before docking calculations, the LigPrep tool was used to generate the 2D and 3D conformations for the ligands [41]. Then hydrogen atoms were added following the adjustment of atoms charges, as well as Epik tool was used to generate the ionization states at pH 7.0 ± 1.0 [42]. Ligand conformations were generated using the OPLS3e force field using the default settings [43]. Poses were investigated and chosen based on the native ligands 40 L and PTR. Then, selected poses with higher binding affinities were submitted to molecular dynamic simulations to study the stability of their binding interactions with the active sites. The resulting docking outcomes were visualized using Biovia Discovery Studio 2020 software [44], followed by an analysis of the docking results.

2.6.2. Molecular dynamics simulation and free energy calculations

MD simulation method was used to analyze the dynamic motion of the compounds **7** and **10** in a complex with phosphoinositide 3-kinases (PI3k δ), pdb: 4xe0, and tyrosine phosphatase PTPRC(CD45) pdb: 1ygr, for 200 nanosecond simulation time [45]. The simulations were conducted using the maestro-Desmond software program with the OPLS3e force field [46,47], in a periodic cell boundary condition as an orthorhombic box, and the SPC water solvation method at 300 K. System energy was reduced, and generated using salt in such a precise concentration of Na⁺ and Cl charge was provided. Temperature and pressure were adjusted using a Nose-Hoover chain thermostat maintaining a temperature of 300 K, and the pressure was maintained at 1.01 bar with Martyna-Tobias-Klein barostat. MD simulations were performed for 1 ns simulation runs under NVT at 300 K, followed by 100 ns under NPT ensemble. Finally, the results of the MD trajectories were analysed to determine root mean square deviation (RMSD), Root Mean Square Fluctuation (RMSF), and protein-ligand interaction.

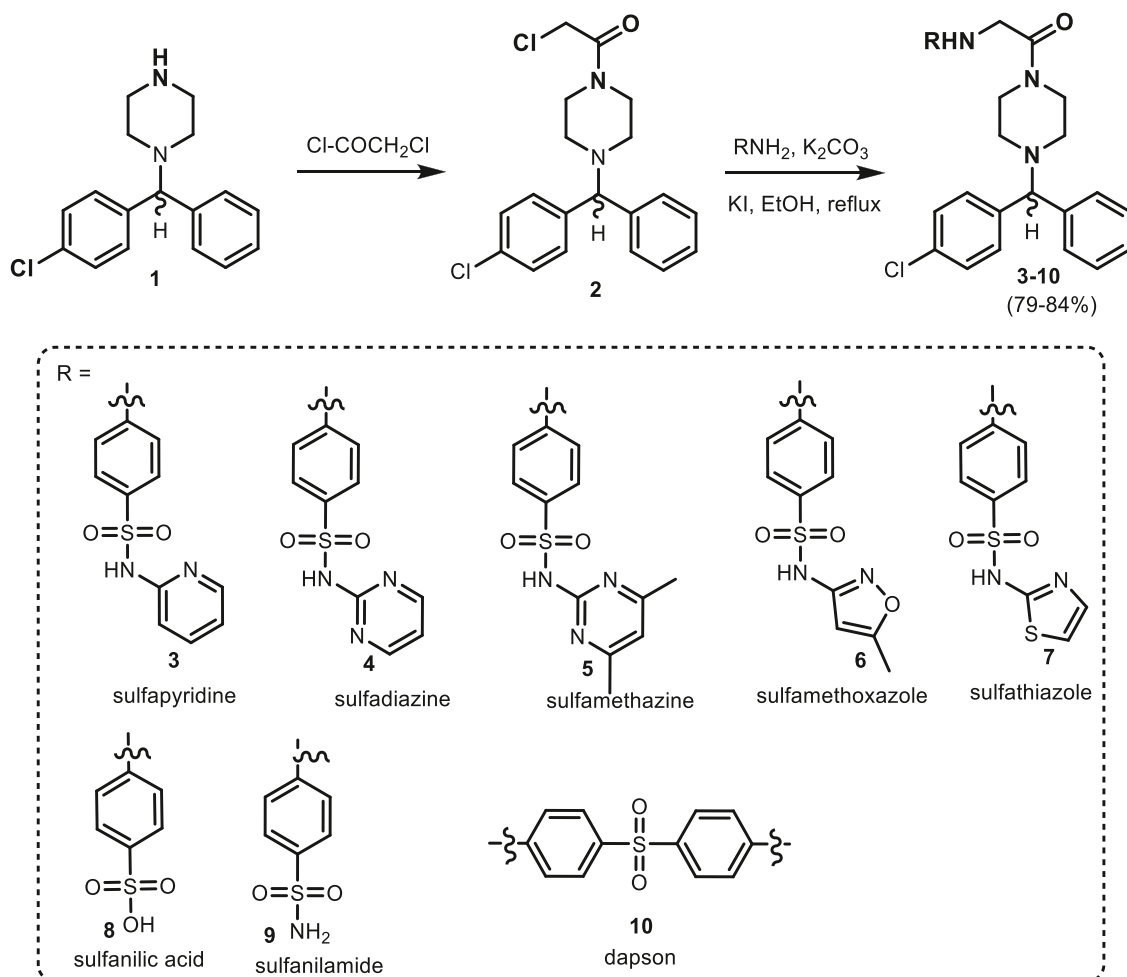
2.7. DFT calculations

All DFT calculations were done using Gaussian 16 software [48]. The electronic structures of the studied compounds were freely geometry optimized in the gas phase using B3LYP [49] hybrid functional assisted with the 6–31+G(d,p) split-valence Pople basis set. To ensure that the calculated structures are global minima on the potential energy surface, the vibrational frequencies were also calculated at the same level of theory as with the optimization. The absence of imaginary frequencies was taken as evidence of the stability of the calculated structure.

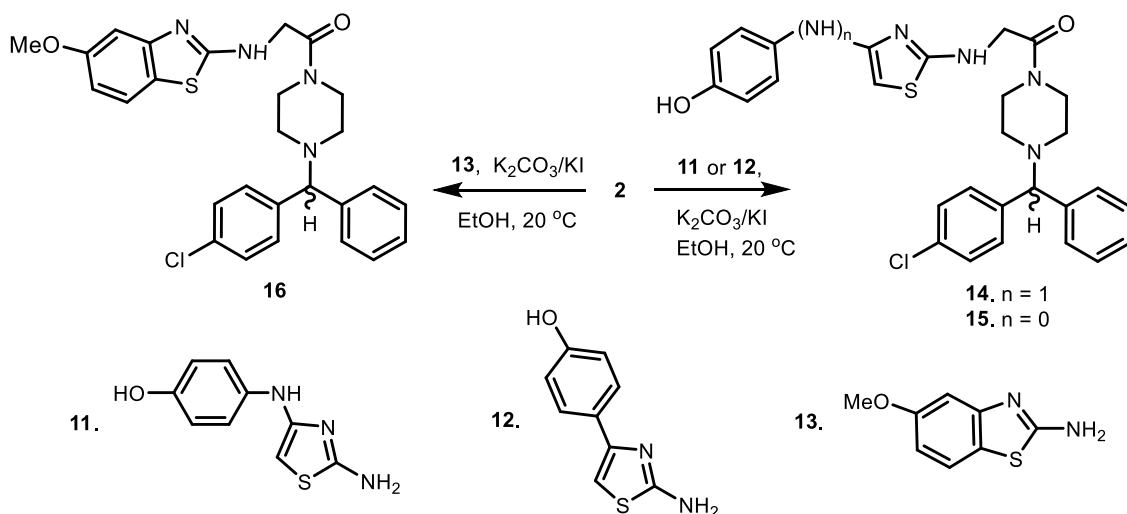
3. Results and discussion

3.1. Chemistry

1-(4-Chlorobenzhydryl) piperazine (**1**) scaffold has been selected as a key intermediate for the synthesis of novel 1-(4-chlorobenzhydryl) piperazine derivatives bearing sulfa drugs and thiazole precursors. Thus, treatment of **1** with chloroacetyl chloride in the presence of base afforded the acyl chloride analogue **2** (68 %). Reaction of **2** with various sulfa drugs such as: sulfapyridine, sulfadiazine, sulfamethazine, sulfamethoxazole, sulfathiazole, sulfanilic acid and sulfanilamide in the presence of K₂CO₃/KI afforded 4-[(4-chlorophenyl)phenylmethyl]-N-(4-(arylsulfamoyl)phenyl) piperazine-1-carboxamide derivatives **3–9** in 79–84 % yield. Analogously, treatment of 2.0 mole of compound **2** with 1.0 mole of dapson in the presence of the same reagents gave the bis-benzhydryl piperazine-dapsone **10** in 85 % yield (Scheme 1).



Scheme 1. Synthesis of some novel 1-(4-chlorobenzhydryl) piperazine bearing sulfa drugs and dapson moiety.



Scheme 2. Synthesis of some novel benzhydryl piperazine conjugated thiazole precursors.

The structures of 3–10 were assigned on the basis of their IR, ¹H, ¹³C and 2D NMR spectra, since they showed similar patterns of aromatic protons and carbon atoms and are presented in Supplementary data (Figs. S1–S24). In the ¹H NMR spectra of 3–10, the benzyl protons appeared as singlets in the region δ 3.43–3.92 ppm whereas the bridge protons were resonated as singlets in the region δ 4.84–5.73 ppm. The

broad singlets or multiplets in the region δ 2.73–3.86 ppm were assigned to the eight piperazine protons. H-3', H-5' and H-6' of pyridine ring of 3 appeared as multiplets or doublet of doublets at δ 6.56, 6.70 and 8.10 (*J* = 7.9, 3.5 Hz) ppm, respectively, while H-5' and H-2'+H-6' of compound 4 resonated as multiplets at δ 7.05 and 8.34 ppm, respectively. In addition, H-5', H-4' and H-5' of 5–7 were resonated as singlets at δ 7.07,

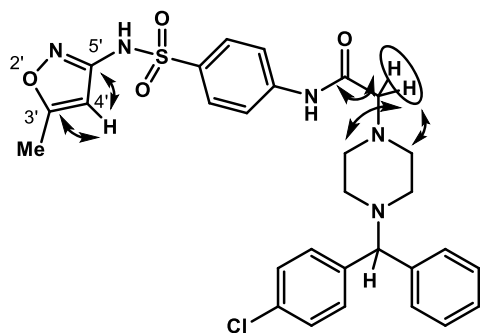


Fig. 1. $J_{C,H}$ correlations in the NMR HMBC correlations of 6.

Table 1

In vitro anticancer activity against a broad panel of cancer cell lines.

Comp.	IC ₅₀ (μM)						
	Capan-1	HCT-116	LN229	DND-41	HL-60	K562	Z138
3	> 100	> 100	> 100	> 100	> 100	> 100	> 100
4	51.6	> 100	> 100	45.95	48.10	84.70	48.95
5	46.3	> 100	> 100	43.95	43.00	> 100	46.45
6	93.90	> 100	> 100	45.25	92.30	> 100	39.80
7	33.35	> 100	> 100	22.00	47.85	> 100	6.85
8	55.50	> 100	94.80	46.35	38.75	62.20	41.70
9	42.15	23.10	46.75	39.75	38.73	53.15	42.00
10	42.80	> 100	44.30	7.40	34.75	> 100	32.15
ETP	0.45	1.02	2.40	2.80	0.40	1.44	0.60
NDZ	0.09	1.45	2.40	0.45	0.10	0.07	0.30

ETP: Etoposide, NDZ: Necodazole.

6.32 and 6.80 ppm, respectively.

The other aliphatic and aromatic protons have been fully analysed (c.f. Experimental section). In the ¹³C NMR spectra of 3–10, resonances in the region δ 56.5–45.2 ppm were assigned to benzyl carbon atom, whereas the signals at δ 74.1–73.9 ppm were belonged to the bridged carbon atom. Piperazine carbons atoms appeared in the region δ 51.8–44.0 ppm. The other carbon atoms of aliphatic and aryl groups have been fully analysed (c.f. Experimental section).

Next, treatment of the key intermediate 2 with 4-((2-aminothiazol-4-yl)amino)phenol (11), 4-((2-aminothiazol-4-yl)phenol (12) or 2-amino-5-methoxybenzothiazole (13) in the presence of K₂CO₃ and KI gave compounds 14–16 in 78, 74 and 79 % yield, respectively (Scheme 2).

The structures of 14–16 were confirmed by their IR, ¹H and ¹³C NMR. The benzhydryl piperazine protons showed a similar pattern

Table 2

Antioxidant activity of new 1-(4-chlorobenzhydryl)piperazine analogues 3–10, and 14–16.

Compd.	% Inhibition conc.										
	1000	900	800	700	600	500	250	125	62.5	31.25	
3	86.5	85.4	82.6	81.2	81.1	77.1	72.7	66.9	63.0	56.9	
4	86.5	85.4	82.6	81.2	80.1	72.7	66.9	63.5	60.5	54.4	
5	95.0	93.9	92.5	91.4	85.4	72.7	66.9	63.5	60.5	54.5	
6	93.1	84.8	69.6	59.9	54.7	48.3	23.2	20.4	18.0	16.9	
7	96.4	96.1	95.6	93.2	92.3	90.9	87.6	84.8	78.5	75.7	
8	79.0	74.3	63.5	61.6	60.8	47.8	42.0	23.2	6.1	0.0	
9	94.2	93.1	85.4	81.5	79.0	75.4	73.2	69.6	63.0	57.2	
10	79.0	76.8	74.6	72.7	66.9	59.9	52.8	47.5	32.3	6.1	
14	35.6	33.7	31.2	29.6	26.2	18.2	14.4	11.6	5.8	3.0	
15	16.9	3.3	0.6	0.0	0.0	0.0	0.0	0.0	0.0	0.0	
16	80.4	76.5	73.5	71.5	63.0	57.5	55.5	48.1	47.0	32.9	
A.A.	99.7	99.2	98.3	98.1	97.5	97.2	96.1	95.3	94.8	93.6	

A.A. = Ascorbic acid.

(Figs. S25–S32). In the ¹H NMR spectra of 14–16, the eight protons of piperazine were observed as multiplets within chemical shift range of δ_H 2.94 and 3.90 ppm, while CH₂ resonated as singlets at δ_H 3.90 and 3.57 (2) ppm, respectively. H_{bridge} appeared as singlets at δ_H 5.45, 5.72 and 5.38 ppm, respectively. Additionally, H-5 of the thiazole ring of 14 and 15 was observed as singlets at δ_H 5.72 and 7.09 ppm, respectively. The aliphatic and aromatic protons were fully analysed (c.f. Experimental section). In the ¹³C NMR spectra of 14–16, the carbonyl carbon atoms (C=O) resonated within the range δ_C 168.4–172.5 ppm, while the resonances at δ_C 162.5, 166.9 and 170.4 ppm assigned to the C-2 of the thiazole ring, respectively. The resonances at δ_C 153.4, 153.1 and 106.0 ppm were assigned to C-4 of the thiazole or benzothiazole moieties, respectively, whereas C-5 of the same moieties was observed at δ_C 104.1, 110.7 and 154.8 ppm, respectively. In addition, the bridge carbon atoms were detected at δ_C 74.1 and 73.9 (2) ppm. The CH₂ carbon atoms resonated at δ_C 60.5 ppm, and the piperazine carbon atoms were observed in the range δ_C 45.1 and 51.8 ppm. The other aromatic and aliphatic substituents carbon atoms were fully analysed (c.f. Experimental section).

Compound 6 was selected for further NMR experiment. In the gradient-selected HMBC spectrum [50] NMR spectrum of 6 showed two ³J_{C,H} heteronuclear correlations of CH₂ protons at δ_H 3.56 ppm with piperazine carbon atoms at δ_C 51.8 ppm. Additional CH₂ protons revealed a ³J_{C,H} correlation with the carbonyl carbon atom at δ_C 164.9 ppm. Moreover, two ²J_{C,H} correlations between H-4' of isoxazole ring at 6.32 ppm with both carbon atoms C-3 and C-5' of isoxazole moiety at δ_C 170.5 and 95.8 ppm, respectively were observed (Fig. 1).

3.2. Biological activity

3.2.1. *In vitro* anticancer screening

The newly synthesized compounds 3–10 have been selected for screening of their anticancer activity on a diverse selection of human cancer cell lines: Capan-1-pancreatic adenocarcinoma, HCT-116-colorectal carcinoma, LN-229-glioblastoma, NCI-H460-lung carcinoma, DND-41-acute lymphoblastic leukemia, HL-60-acute myeloid leukemia, K-562-chronic myeloid leukemia, H and Z-138-non-Hodgkin lymphoma cancer cells (Table 1) using MTS assay [40]. For comparison purposes, etoposide, and necodazole were used as references standard. Table 1 demonstrated that compound 7 emerged as the most potent compound within the series. It demonstrated an IC₅₀ value of 6.85 μM against the Z-138 cancer cell line, and an IC₅₀ value of 22.00 μM against the DND-41 cancer cell line. Additionally, compound 10 exhibited an IC₅₀ value of 7.40 μM against the DND-41 cancer cell lines, while displaying IC₅₀ values of 32.15 μM and 34.75 μM against the Z138 and HL-60 cell lines, respectively. Furthermore, compounds 8 and 9 demonstrated IC₅₀ values of 38.75 μM and 38.73 μM, respectively, against the HL-60 and DND-41 cancer cell lines, respectively.

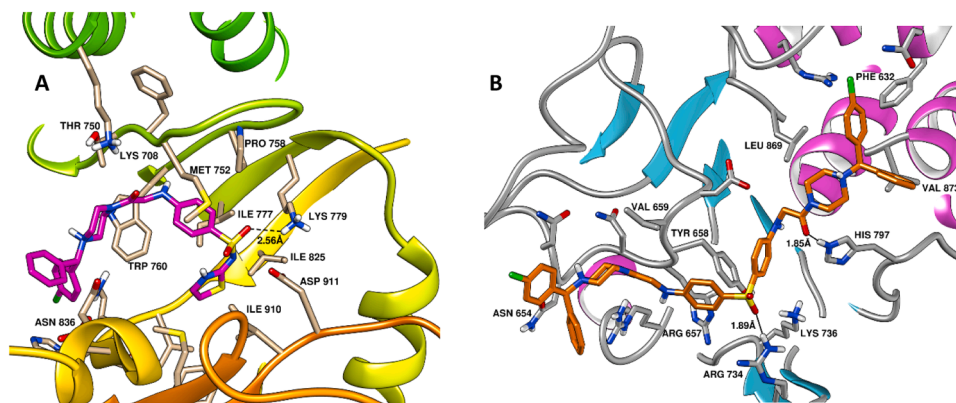


Fig. 2. The docking poses of the compounds (A) compound **7** and (B) compound **10** in the phosphoinositide 3-kinases (PI3k δ) and tyrosine phosphatase active sites (PDB ID's: 4xe0 and 1ygr, respectively). The important amino acid residues involved in the polar and non-polar interactions are highlighted.

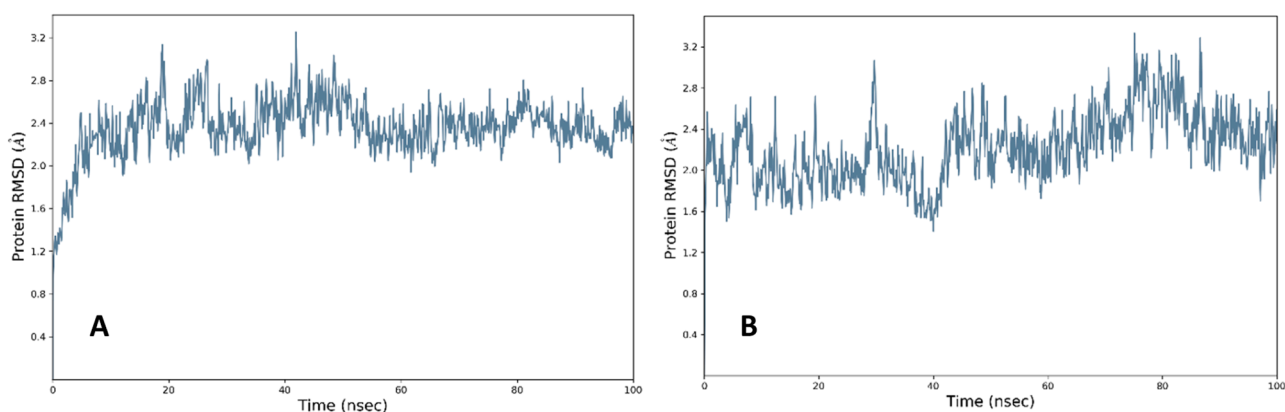


Fig. 3. RMSD values of backbone atoms of compounds **7** (A), and compound **10** (B) in complex with phosphoinositide 3-kinases (PI3k δ) and tyrosine phosphatase active sites (PDB ID's: 4xe0 and 1ygr, respectively).

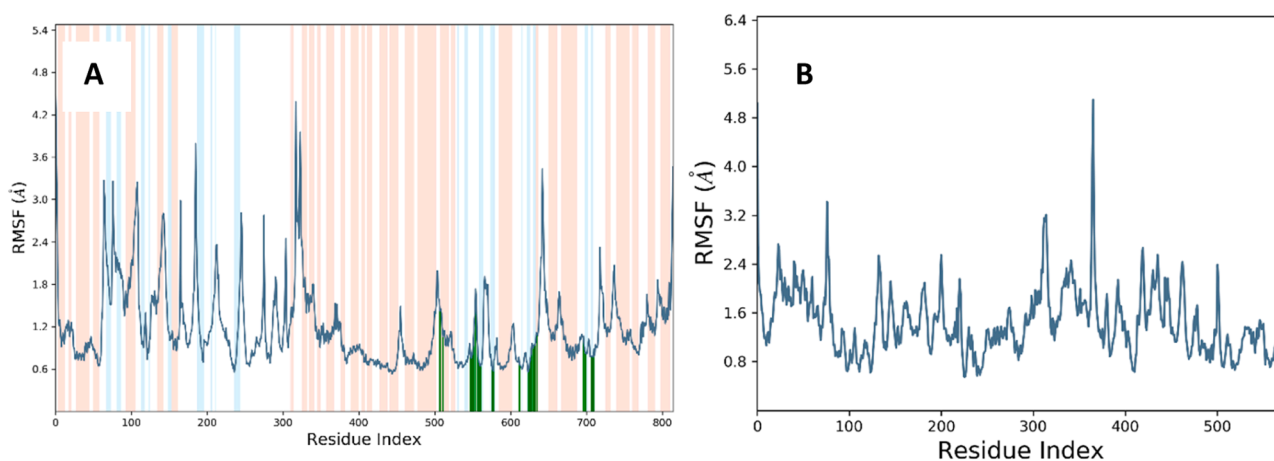


Fig. 4. RMSF profiles of the compounds. ((A) compound **7**, (B) compound **10** (B), with phosphoinositide 3-kinases (PI3k δ) and tyrosine phosphatase active sites, respectively).

The SAR study indicated that the anticancer activity of compounds **3–10** was influenced by the substituents of the aryl amide ring. Specifically, compound **7**, which featured a thiazole-sulfonamide substituent at the para position of the phenyl-amide ring, exhibited the most potent antitumoral activity, particularly against the Z138 cancer cell line. Moreover, compound **10** with a dapson moiety centered between two benzhydryl piperazine backbones, showed nearly comparable antitumoral activity to compound **7** against the DND-41 cell line. These

findings provide compelling evidence to explore the synthesis of various substituted thiazole-sulphonamide derivatives, as they have the potential enhance the antiproliferative effects on different cancer cell lines.

3.2.2. Antioxidant activity

The antioxidant activity was performed using DPPH (1,1-diphenyl-2-picrylhydrazyl) radical scavenging assay [51], where ascorbic acid was used as a positive control for comparison. Method is based on the

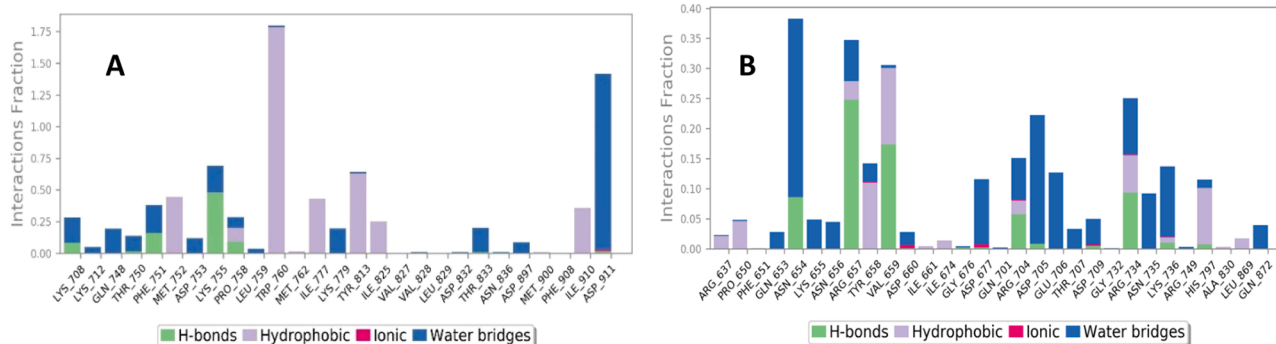


Fig. 5. Ligand-protein contact histogram of compound 7 (A), compound 10 (B), (PDB ID's: 4xe0 and 1ygr, respectively).

Table 3

Total energies, HOMO and LUMO energies, the HOMO-LUMO gaps (in atomic unit), and the dipole moment (in Debye) calculated by the B3LYP/6-31+G(d,p) level of theory in gas phase.

Compd.	E_{Total} (Hartree)	Dipole (Debye)	E_{HOMO} (Hartree)	E_{LUMO} (Hartree)	HOMO-LUMO gap (Hartree)
3	-2519.058381	7.082105	-0.30520	-0.19267	-0.11253
4	-2535.102159	8.297892	-0.30521	-0.19263	-0.11258
5	-2613.752914	8.400610	-0.30518	-0.19268	-0.1125
6	-2556.136520	9.193558	-0.30541	-0.19138	-0.11403
7	-2839.821056	10.169429	-0.29203	-0.19263	-0.0994
8	-2291.839515	8.974026	-0.30533	-0.19235	-0.11298
9	-2271.962831	9.076055	-0.30528	-0.19251	-0.11277
10	-3883.439615	8.520905	-0.30534	-0.19230	-0.11304
14	-3146.109177	10.143087	-0.28604	-0.19253	-0.09351
15	-3201.453482	10.274079	-0.26852	-0.19261	-0.07591
16	-2273.024582	2.868279	-0.28115	-0.19253	-0.08862

reduction of DPPH radicals solution in the presence of hydrogen donating antioxidant, due to the formation of the non-radical form DPPH-H. The results of antioxidant activity of compounds 3–10, and 14–16 are shown in Table 2. The radical scavenging was expressed in terms of % inhibition at various concentrations 1000, 900, 800, 700, 600, 500, 250, 125, 62.5 and 31.25 μM which denotes the concentration required to scavenge 50 % of DPPH radicals. As shown in Table 2, almost all compounds had low or no antioxidant activity in the DPPH assay. The % inhibition concentration in the DPPH assays was in the range of 0–75.7 μM DPPH at a solution concentration of 31.25 μM . Compound 7 exhibited highest antioxidant activity with inhibition of 75.7 % at a concentration of 31.25 μM and 96.4 % at a concentration of 1000 μM compared to the standard ascorbic acid (93.6 and 99.7 %, respectively). Compound 9 with sulfanilamide group exhibited antioxidant activity (57.2 %) higher than compounds 3–5 with inhibition of 56.9, 54.4 and 54.5 %, respectively.

In particular, DPPH scavenging activity, only 7 demonstrated the almost high activity among the series. The activity fully based upon the presence of the thiazole moiety at end of the integrated sulfonamide scaffold. The other substituents like pyridine, and pyrimidines, tolyl, propyl and methyl made the compounds moderate active. Therefore, analogue 7 could be considered as a lead compound for further development for the DPPH scavenging activity

4. Molecular docking study

The objective of molecular docking calculations is to forecast the most probable interaction mechanism between a protein and a ligand [52]. Molecular docking of the synthesized compounds 7 and 10 were studied with the active sites of the phosphoinositide 3-kinases (PI3k δ) and tyrosine phosphatase PTPRC(CD45) PDB ID: 4xe0 and 1ygr,

respectively. The prospective ligands were ranked according to the highest affinity of the best conformers. The calculated Glide binding energy score for compound 7 is $-7.35 \text{ kcal/mol}^{-1}$ (rmsd = 1.390), and for compound 10 is $-6.84 \text{ kcal/mol}^{-1}$ (rmsd = 1.420), respectively, indicating selectivity binding of this analogue to the active site of the protein receptors.

Fig. 2(A) showed the docking of compound 7 oriented in an appropriate position for its binding with the protein receptors of phosphoinositide 3-kinases (PI3k δ) via a hydrogen bond between O-32 and O-33 of the sulfone moiety and Lys779 with a distance of 2.56 Å. It can be observed that compound 7 forms various hydrophobic interactions with Thr750, Trp760, Met752, Pro758, Ile777, Ile825, and Ile910 amino acid residues. Fig. 2(B) revealed the docking results of compound 10 with the tyrosine phosphatase PTPRC(CD45) (PDB: 1ygr). It showed two hydrogen bonds, the first one between O-3 of the carbonyl moiety and His797 with a 1.85 Å distance, and the second H-bond between O-32 and O-33 of the sulfone moiety and Arg734 with the distance of 1.89 Å. This study suggests that the main factor that contributes to the stabilization of the receptor-inhibitor complexes is hydrophobic interactions.

5. Molecular dynamics simulation

Molecular dynamics simulation was utilized to study the stability of phosphoinositide 3-kinases (PI3k δ) (4XE0) and tyrosine phosphatase PTPRC(CD45) (1YGR) inhibitors, labelled as 7 and 10, respectively. The simulations spanned a duration of 200 ns, during which the dynamic stability and intermolecular interactions of the docked protein-ligand complexes were analysed. To assess the outcomes of each system over the 100 ns period for each system, various parameters such as protein-ligand root mean square deviation (RMSD), protein root mean square fluctuation (RMSF), and protein-ligand interactions were employed.

5.1. Protein-Ligand root mean squared deviation (RMSD)

The Root Mean Square Deviation (RMSD) is used to measure the average change in displacement of a selection of atoms for a particular frame with respect to a reference frame. It is calculated for all frames in the trajectory. The RMSD for frame x is:

$$RMSD_x = \sqrt{\frac{1}{N} \sum_{i=1}^N (r'_i(t_x) - r_i(t_{ref}))^2}$$

where N is the number of atoms in the atom selection; t_{ref} is the reference time, (typically the first frame is used as the reference and it is regarded as time $t = 0$); and r' is the position of the selected atoms in frame x after superimposing on the reference frame, where frame x is recorded at time t x. The procedure is repeated for every frame in the simulation trajectory. The RMSD value of complex 7 was determined and found to be between 0.15 and 0.25 nm with an average of 0.24 nm. On the other hand, complex 10 shows an increase in RMSD value from

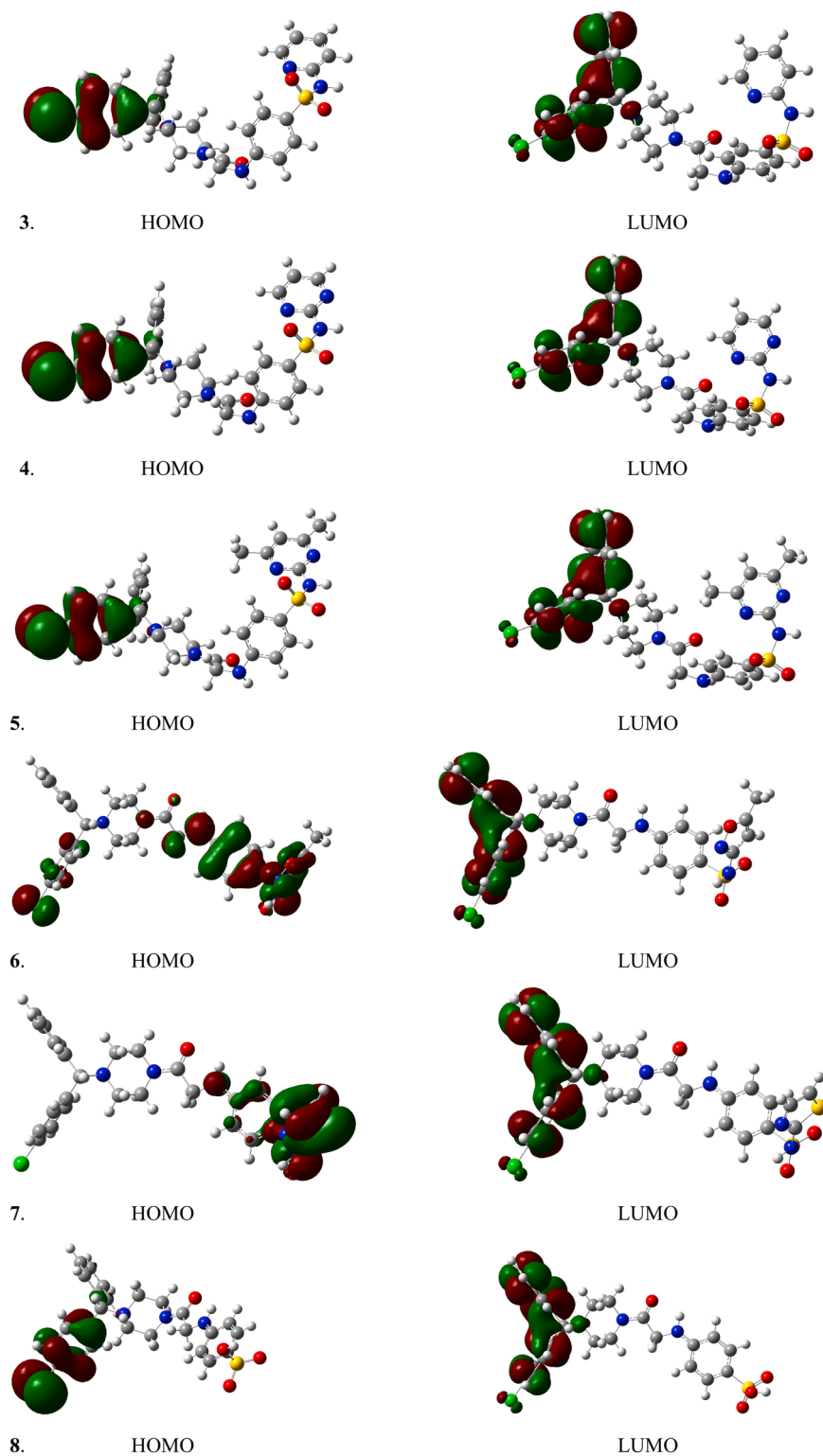


Fig. 6. The frontier orbitals of the studied molecules 3–10, and 14–16.

(0.16 nm–0.32 nm) in the last 50 ns as shown in Fig. 3. This result indicates that complex 7 promotes higher stability within the phosphoinositide 3-kinases (PI3k δ) active site, and reflects the less stability of the bulky compound 10 to cause higher conformational changes along the interactions with tyrosine phosphatase active site during the simulation time.

5.2. Protein RMSF

The root mean square fluctuation (RMSF) is analysed to measure the residual fluctuation of amino acids. High RMSF values indicate the flexibility of the amino acids. However, low RMSF values of amino acid residues show the stability of those regions of amino acids in the receptor. Analysis of the highest RMSF values for complex 7 found to be

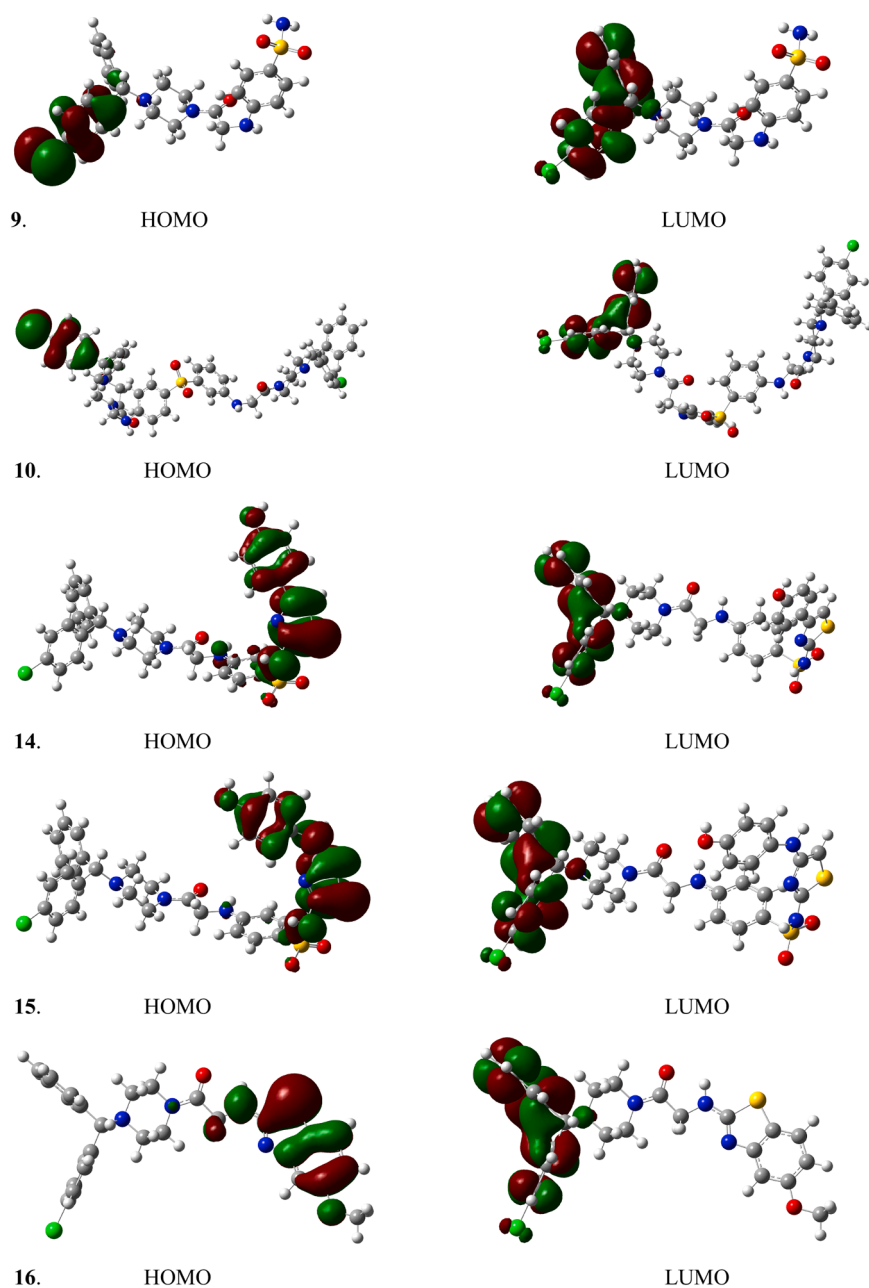


Fig. 6. (continued).

0.34 nm, 0.37 nm, and 0.43 nm, which belong to the loop of the C-terminal of 655–662 (cyan), 197–200 (green), and 317–329 (magenta) amino acid residues, respectively. Whereas the fluctuation profiles in complex **10** are located in the loop residue numbers 70–75, magenta, (0.34 nm) and 370–375, green, (0.49 nm) as shown in Fig. 4.

In general, the fluctuation profiles in complexes **7** and **10** are located in different loops of amino acid residues which have high flexibility. This finding implies the high flexibility of compound **10** during the complexation in the active site of the tyrosine phosphatase *PTPRC* (CD45) receptor due to the bulkiness factor and increasing the number of rotatable bonds.

5.3. Protein-Ligand contact

Fig. 5 shows the number of hydrogen bonds during 100 ns between compounds **7** and **10** with the amino acid residues of the phosphoinositide 3-kinases (PI3k δ) and tyrosine phosphatase *PTPRC*(CD45),

respectively. MD simulations were conducted to examine the protein-ligand interactions in complexes **7** and **10**, and the results are depicted in Fig. 5. The results demonstrate the formation of stable complexes and highlight various intermolecular interactions that contribute to their stability throughout the simulation time. The receptor-ligand complexes exhibit a diverse array of interactions, including hydrophobic interactions, hydrogen bonding, and water-bridge hydrogen bonding interactions. These interactions are crucial for maintaining the stability and integrity of the complexes during the MD simulation. Complex **7**, Fig. 5A, ligand forms both hydrogen bonds and hydrogen-bonded mediated by a water molecule with specific residues such as Lys755, Lys779, and Asp911. In addition, nonpolar interactions form with Trp760, Tyr813, Met752, Ile 777, Ile 910, Ile825, and significant hydrophobic interaction with Trp760 which is in agreement with our docking study. As for the second complex **10**, Fig. 5B, distinct hydrogen bonds are observed with residues Asn654, Arg657, Asp677, Asp705, Arg734, and His797, while hydrophobic interactions are observed with

residues Pro650, Tyr658, Val659, and Leu869. These specific interactions are pivotal for the stability of this complex.

6. DFT calculations

Some of the calculated electronic properties of the studied compounds **3–10**, and **14–16** (including total energies, HOMO and LUMO energies, HOMO-LUMO gaps, and the dipole moments) are listed in Table 3, whereas the frontier orbitals are shown in Fig. 6.

As depicted in Fig. 6, the HOMO energies of compounds **3** to **10** exhibit separation across the chlorobenzene moiety, except for analogues **6** and **7**. These energies are nearly degenerate and fall within the range of -0.30518 to -0.30533 a.u., as shown in Table 3. On the other hand, the LUMO in these molecules is localized above the chlorophenyl ethyl-benzene moiety. For compounds **6** and **7**, the HOMO is situated differently, with compound **6**'s HOMO spanning the isoxazolyl-methylamino-benzenesulfonamide moiety and also extending to cover the chlorobenzene precursor, while compound **7**'s HOMO is centered over the azaneyl-thiazolyl-benzenesulfonamide moiety. The HOMO-LUMO gap energies in these molecules exhibit similar values, with compound **7** having the smallest gap energy. For compounds **14–16**, the LUMO is situated over the chlorophenyl ethyl-benzene moiety, whereas the HOMO is distributed differently. Specifically, for compound **14**, the HOMO covers the azaneyl-thiazolyl-phenol moiety with an energy of -0.28604 a.u. For compound **15**, the HOMO extends over the aminothiazolyl-aminophenol moiety, possessing an energy of -0.26852 a.u. Lastly, for compound **16**, the HOMO is separated over the 5-methoxy-methylbenzothiazolamine moiety, with an energy of -0.28115 a.u. In general, the HOMO-LUMO gap energies of these molecules are smaller compared to compounds **3–10**, with values falling within the range of -0.05859 to -0.09351 a.u. The frontier orbitals of the studied molecules are notably separated, indicating a significant degree of charge transfer. This observation suggests that these molecules could be promising candidates for exhibiting Non-Linear Optical properties

7. Conclusions

In this study, a range of 1-(4-chlorobenzhydryl) piperazine derivatives carrying sulfa drugs and substituted 2-aminothiazole derivatives **3–10**, and **14–16** were synthesized from 1-(4-chlorophenylbenzhydryl) piperazine (**1**) via the key intermediate 1-allyl-4-((4-chlorophenyl) phenylmethyl) piperazine (**2**). Subsequently, the synthesized compounds were subjected to evaluation for their potential antiproliferative activity against seven different human cancer cell lines. Interestingly, derivatives **7** and **10** displayed the most promising activity among the entire series, particularly against the Z-138-non-Hodgkin lymphoma and the DND-41-acute lymphoblastic leukemia, respectively. The study also included an assessment of the antioxidant activity of all the synthesized compounds. Compound **7** showed moderate DPPH scavenging activity, setting it apart from the rest of the series. Additionally, a molecular docking study was conducted on compound **7**, revealing intriguing binding interactions between its substituents and the phosphoinositide 3-kinase (protein PI3k δ) as well as residues of compound **10** with the receptor tyrosine phosphatase PTPRC (CD45). These findings provide valuable insights for designing novel substituted-benzhydryl piperazine analogues with significant potential as anticancer agents, as well as for guiding future structural modifications. In addition, the molecular dynamics simulation of compounds **7** and **10** has been studied. The density functional theory (DFT) has been applied to investigate all the newly synthesized compounds.

Appendix A. Supplementary data

Supplementary data related to this article can be found at <https://doi.org/10.1016/j.molstruc.2023.137028>.

CRediT authorship contribution statement

Najim A. Al-Masoudi: Conceptualization, Supervision, Methodology, Project administration, Visualization. **Raad S. Jihad:** Investigation. **Nabeel A. Abdul-Rida:** Methodology, Resources. **Amer M.J. Al-Shamari:** Methodology, Resources. **Bahjat A. Saeed:** Formal analysis. **Wasfi A. Al-Masoudi:** Investigation. **Amneh Shtaiwi:** Formal analysis. **Yaseen A. Al-Soud:** Methodology.

Declaration of Competing Interest

The authors declare the following financial interests/personal relationships which may be considered as potential competing interests: Najim A. Al-Masoudi reports administrative support and equipment, drugs, or supplies were provided by University of Basrah. Najim A. Al-Masoudi reports a relationship with University of Basrah that includes: non-financial support. If there are other authors, they declare that they have no known competing financial interests or personal relationships that could have appeared to influence the work reported in this paper.

Data availability

No data was used for the research described in the article.

Acknowledgments

We acknowledge Leentje Persoons and Dirk Daelemans from the Laboratory of Virology and Chemotherapy, KU Leuven, Belgium for the antitumoral testing of the compounds.

Supplementary materials

Supplementary material associated with this article can be found, in the online version, at [doi:10.1016/j.molstruc.2023.137028](https://doi.org/10.1016/j.molstruc.2023.137028).

References

- [1] C. Siddegowda, A. Kumar, K. Murthy, M.P. Sadashiva, M.K. Vinaya, N. R. Thimmegowda, S.B.B. Prasad, S. Chandrappa, K.S. Rangappa, Synthesis and in vitro antimicrobial activity of medicinally important novel N-alkyl, N-aryl and urea derivatives of 1-benzhydryl piperazine: a structure activity relationship study, *Lett. Drug Design Discov.* 6 (2009) 146–154, <https://doi.org/10.2174/157018009787582570>.
- [2] C.S.A. Kumar, K. Vinaya, J.N.S. Chandra, N.R. Thimmegowda, S.B.B. Prasad, C. T. Sadashiva, K.S. Rangappa, Synthesis and antimicrobial studies of novel 1-benzhydryl-piperazine sulfonamide and carboxamide derivatives, *J. Enz. Inh. Med. Chem.* 23 (2008) 462–469, <https://doi.org/10.1080/14756360701654969>.
- [3] L.L.B. Fang, C.H. Zhou, Synthesis of azole-containing piperazine derivatives and evaluation of their antibacterial, antifungal and cytotoxic activities, *Bull. Korean Chem. Soc.* 31 (2010) 3684–3692, <https://doi.org/10.5012/BKCS.2010.21.12.3684>.
- [4] J.N.N.S. Chandra, C.T. Sadashiva, C.V. Kavitha, K.S. Rangappa, Synthesis and in vitro antimicrobial studies of medicinally important novel N-alkyl and N-sulfonyl derivatives of 1- [bis(4-fluorophenyl)-methyl] piperazine, *Bioorg. Med. Chem.* 14 (2006) 6621–6627, <https://doi.org/10.1016/j.bmc.2006.05.064>.
- [5] S. Shivaprakash, K.R. Kiran, L. Diwakar, G.C. Reddy, Synthesis and in-vitro study of novel (Z)-1-benzhydryl-4-cinnamylpiperazine derivatives as potential anticancer agents, *Int. J. Pharm. Pharm. Sci.* 7 (2014) 416–420.
- [6] R. Khanam, R. Kumar, I.I. Hejazi, S. Shahabuddin, R. Meena, P. Rajamani, N. Yadav, A.I. Bhat, F. Athar, New N-benzhydryl piperazine/1,3,4-oxadiazoles conjugates inhibit the proliferation, migration, and induce apoptosis in HeLa cancer cells via oxidative stress-mediated mitochondrial pathway, *J. Cell. Biochem.* 120 (2019) 1651–1666, <https://doi.org/10.1002/jcb.27472>.
- [7] D. Ruzic, B. Ellinger, N. Djokovic, J.F. Santibanez, S. Gul, M. Beljkas, A. Djuric, A. Ganesan, A. Pavic, T. Srdic-Rajic, M. Petkovic, K. Nikolic, Discovery of 1-benzhydryl-piperazine-based HDAC inhibitors with anti-breast cancer activity: synthesis, molecular modeling, in vitro and in vivo biological evaluation, *Pharmaceutics* 14 (2022) 2600–2624, <https://doi.org/10.3390/pharmaceutics14122600>.
- [8] M.R. Cuberes-Altsient, J. Frigola-Constansa, J. Pares-Corominas, Derivatives of 1-diphenyl Methyl Piperazine and Their Use As Antihistamines, US Patent, 1992, 5, 166,205.

- [9] A. Ahmadi, M. Khalili, A. Nafarie, A. Yazdani, B. Nahri-Niknafs, Synthesis and anti-inflammatory effects of new piperazine and ethanolamine derivatives of H1-antihistaminic drugs, *Mini Rev. Med. Chem.* 12 (2012) 1282–1292, <https://doi.org/10.2174/138955712802762013>.
- [10] S.J. Rhee, Y.L. Kam, Y.H. Seo, H.Y.P. Choo, Antihistamine activities of iminodiacetamide derivatives, *Biomol. Therap.* 16 (2008) 416–424, <https://doi.org/10.4062/biomolther.2008.16.4.416>.
- [11] L. Wang, T. Wang, B. Yang, Z. Chen, H. Yang, Design, synthesis, and antiallergic activities of novel (R)-(-)-1-[(4-chlorophenyl)phenylmethyl]piperazine derivatives, *Med. Chem. Res.* 21 (2010) 124–132, <https://doi.org/10.1007/s00044-010-9512-1>.
- [12] J.H. Chern, K.S. Shia, T.A. Hsu, C.L. Tai, C.C. Lee, Y.C. Lee, C.S. Chang, S.N. Tesng, S.R. Shih, Design, synthesis, and structure-activity relationships of pyrazolo[3,4-d]pyrimidines: a novel class of potent enterovirus inhibitors, *Bioorg. Med. Chem.* 14 (2004) 2519–2525, <https://doi.org/10.1016/j.bmc.2004.02.092>.
- [13] F. Curreli, H. Zhang, X. Zhang, I. Pytkin, Z. Vitor, A. Altieri, A.K. Debnath, Virtual screening based identification of novel small-molecule inhibitors targeted to the HIV-1 capsid, *Bioorg. Med. Chem.* 19 (2011) 77–90, <https://doi.org/10.1016/j.bmc.2010.11.045>.
- [14] A. Santhoshi, N.K. Simgam, S. Pombala, Y. Poornachandra, P.S. Sadhu, C. G. Kumar, J.R. Vaidya, Synthesis of 1-benzhydryl piperazine derivatives and evaluation of their ACE inhibition and antimicrobial activities, *Med. Chem. Res.* 23 (2014) 3207–3219, <https://doi.org/10.1007/s00044-013-0895-7>.
- [15] G.W. Zamponi, Z.P. Feng, L. Zhang, Ho. Pajouhesh, Y. Ding, F. Belardetti, H. Pajouhesh, D. Dolphin, L.A. Mitscher, T.P. Snutch, Scaffold-based design and synthesis of potent N-type calcium channel blockers, *Bioorg. Med. Chem. Lett.* 19 (2009) 6467–6472, <https://doi.org/10.1016/j.bmc.2009.09.008>.
- [16] S. Gubert, M.A. Braso, A. Sacrista, J.A. Ortiz, Synthesis of some N-benzhydryl piperazine derivatives as calcium antagonists, *Arzneimittel-Forsch. (Drug Res.)* 37 (1987) 1103–1107.
- [17] N. Miyake, R. Fujita, M. Ishikawa, M. Takayanagi, K. Sasaki, Reversal of multidrug resistance in human leukemia K562 by tamolarizine, a novel calcium antagonist, *Jpn. J. Pharmacol.* 82 (2000) 265–268, <https://doi.org/10.1254/jip.82.265>.
- [18] H. Pajouhesh, Z.P. Feng, Y. Ding, L. Zhang, Ho. Pajouhesh, J.L. Morrison, F. Belardetti, E. Tringham, E. Simonson, T.W. Zamponi, L.A. Mitscher, T.P. Snutch, Structure-activity relationships of diphenylpiperazine N-type calcium channel inhibitors, *Bioorg. Med. Chem. Lett.* 20 (2010) 1378–1383, <https://doi.org/10.1016/j.bmc.2010.01.008>.
- [19] Y.L. Kam, H.K. Rhee, H. Rhim, S.K. Back, H.S. Na, H.Y.P. Choo, Synthesis and T-type calcium channel blocking activity of novel diphenyl piperazine compounds, and evaluation of in vivo analgesic activity, *J. Bioorg. Med. Chem.* 18 (2010) 5938–5944, <https://doi.org/10.1016/j.bmc.2010.06.082>.
- [20] B.C. Sasse, U.R. Mach, J. Leppaenen, T. Calmels, H. Stark, Hybrid approach for the design of highly affine and selective dopamine D-3 receptor ligands using privileged scaffolds of biogenic amine GPCR ligands, *Bioorg. Med. Chem.* 15 (2007) 7258–7273, <https://doi.org/10.1016/j.bmc.2007.08.034>.
- [21] C.S.A. Kumar, S.B. Prasad, K. Vinaya, S. Chandrappa, N.R. Thimmegowda, Y.C. S. Kumar, S. Swarup, K.S. Rangappa, Synthesis and in vitro antiproliferative activity of novel 1-benzhydryl-piperazine derivatives against human cancer cell lines, *Eur. J. Med. Chem.* 44 (2009) 1223–1229, <https://doi.org/10.1016/j.ejmech.2008.09.025>.
- [22] M. Yarim, M. Koksall, I. Durmaz, R. Atalay, Cancer cell cytotoxicities of 1-(4-substitutedbenzoyl)-4-(4-chlorobenzhydryl)piperazine derivatives, *Int. J. Mol. Sci.* 13 (2012) 8071–8085, <https://doi.org/10.3390/ijms13078071>.
- [23] C.S.A. Kumar, N.S. Shivananju, N.R. Thimmegowda, S.B.B. Prasad, G.W. Yip, K. S. Rangappa, Synthesis and evaluation of 1-benzhydryl-sulfonyl-piperazine derivatives as inhibitors of MDA-MB-231 human breast cancer cell proliferation, *Med. Chem. Res.* 16 (2007) 179–187, <https://doi.org/10.1007/s00044-007-9022-y>.
- [24] L.L. Gan, H.Z. Zhang, C.H. Zhou, Design, Synthesis and relational biological evaluation of novel diphenylpiperazine 1,2,3-triazole derivatives, *Indian J. Pharm. Sci.* 80 (2018) 1045–1046, <https://doi.org/10.4172/pharmaceutical-sciences>.
- [25] E.E. Gurdal, M. Yarim, I. Durmaz, R. Cetin-Atalay, Cytotoxic activities of some novel benzhydryl piperazine derivatives, *Drug Res.* 63 (2013) 121–128, <https://doi.org/10.1055/s-0032-1333275>.
- [26] Z. Rajic, B. Zorc, S. Raic-Malic, K. Ester, M. Kralj, K. Pavelic, J. Balzarini, E. De Clercq, M. Mintas, Hydantoin derivatives of L- and D-amino acids: synthesis and evaluation of their antiviral and antitumor activity, *Molecules* 11 (2006) 837–848, <https://doi.org/10.3390/11110837>.
- [27] D.D. da Silva, M.J. Silva, P. Moreira, M.J. Martins, M.J. Valente, F. Carvalho, M.de L. Bastos, H. Carmo, In vitro hepatotoxicity of 'Legal X': the combination of 1-benzhydryl piperazine (BZP) and 1-(m-trifluoromethylphenyl) piperazine (TFMPP) triggers oxidative stress, mitochondrial impairment and apoptosis, *Arch. Toxicol.* 19 (2017) 1413–1430, <https://doi.org/10.1007/s00204-016-1777-9>.
- [28] I. Valkova, A. Zlatkova, K. Nedza, I. Doytchinova, Synthesis, 5-HT1A and 5-HT2A receptor affinity and QSAR study of 1-benzhydryl-piperazine derivatives with xanthine moiety at N4, *Med. Chem. Res.* 21 (2012) 477–486, <https://doi.org/10.1007/s00044-011-9555-y>.
- [29] V.S. Murthy, Y. Tamboli, V.S. Siva Krishna, D. Seriram, F.X. Zhang, G.W. Zamponi, V. Vijayakumar, Synthesis and biological evaluation of novel benzhydryl piperazine-coupled nitrobenzenesulfonamide hybrids, *ACS Omega* 6 (2021) 9731–9740, <https://doi.org/10.1021/acsomega.1c00369>.
- [30] D. Roy, G. Panda, Benzhydryl amines: synthesis and their biological perspective, *ACS Omega* 5 (2020) 19–30, <https://doi.org/10.1021/acsomega.9b03090>.
- [31] A. Shatawi, R. Adnan, M. Khairuddean, S.U. Khan, Computational investigations of the binding mechanism of novel benzophenone imine inhibitors for the treatment of breast cancer, *RSC Adv.* 9 (2019) 35401–35416, <https://doi.org/10.1039/C9RA04759J>.
- [32] M. Zahid, K.A. Yasin, T. Akhtar, N.H. Rama, S. Hameed, N.A. Al-Masoudi, Synthesis and in vitro antiproliferative activity of new adamantylthiazolyl-1,3,4-oxadiazoles, *Arkivoc* 11 (2009) 85–93, <https://doi.org/10.3998/ark.5550190.0010.b08>.
- [33] Y.A. Al-Soud, H.H. Al-Sa'doni, R.H.M. Al-Shaneek, N.A. Al-Masoudi, P. Loddo, P. L. Colla, Synthesis and in vitro antiproliferative activity of new benzothiazoles derived substituted amido and thiourea piperazine derivatives, *Z. Naturforsch.* 65b (2010) 1372–1380, <https://doi.org/10.1002/chin.201110217>.
- [34] M. Madni, S. Hameed, M.N. Ahmed, N.A. Al-Masoudi, Synthesis, crystal structure, anti-HIV and antiproliferative activity of new pyrazolothiazole derivatives, *Med. Chem. Res.* 26 (2017) 2653–2665, <https://doi.org/10.1007/s00044-017-1963-1>.
- [35] F.A.K. Almashal, H.H. Al-Hujaj, A.M. Jassem, N.A. Al-Masoudi, A click synthesis, molecular docking, cytotoxicity on breast cancer (MDA-MB 231) and anti-HIV activities of new 1,4-disubstituted-1,2,3-triazole thymine derivative, *Russ. J. Bioorganic Chem.* 46 (2020) 360–370, <https://doi.org/10.1134/S1068162020030024>.
- [36] N.A. Abdul-Rida, A.M. Farhan, N.A. Al-Masoudi, B.A. Saeed, D. Miller, M.F. Lin, A novel pregene analogs: synthesis, cytotoxicity on prostate cancer of PC-3 and LNCaP-A1 cells and in silico molecular docking study, *Mol. Divers.* 25 (2021) 661–671, <https://doi.org/10.1007/s11030-020-10038-w>.
- [37] N.A. Abdul-Ridha, A.D. Salmaan, R. Sabah, B. Saeed, N.A. Al-Masoudi, Synthesis, cytotoxicity and in silico study of some novel benzocoumarin-chalcone bearing aryl ester derivatives and benzocoumarin derived arylamide analogs, *Z. Naturforsch.* 76b (2021) 201–210, <https://doi.org/10.1515/znb-2020-0204>.
- [38] Y.A. Al-Soud, A.H. Al-Ahmad, N.A. Al-Masoudi, R.A. Al-Qawasmeh, Synthesis, anticancer activity and molecular docking studies of new 4-nitroimidazole derivatives, *Arkivoc* viii (2021) 296, <https://doi.org/10.24820/ark.5550190.p011.479.-06>.
- [39] H. Bandy, B.A. Saeed, N.A. Al-Masoudi, Synthesis, aromatase inhibitory activity and molecular docking studies of structurally and functionally diverse D-ring pregnenolone pyrazoles, *Anticancer Agents Med. Chem.* 21 (2021) 1671–1697, <https://doi.org/10.2174/1771520620999201124213655>.
- [40] Y. Wang, D.T. Nguyen, G. Yang, J. Anesi, J. Kelly, Z. Chai, F. Ahmady, F. Charchar, J.A. Golledge, A modified MTS proliferation assay for suspended cells to avoid the interference by hydralazine and β-mercaptoethanol, *Assay Drug Dev. Technol.* 19 (2021) 184–190, <https://doi.org/10.1089/adt.2020.1027>.
- [41] Schrödinger Inc, Schrödinger Release 2019 Version 4 Maestro, LigPrep; Schrödinger, LLC, New York, NY, 2019.
- [42] J.C. Shelley, A. Cholletti, L.L. Frye, J.R. Greenwood, M.R. Timlin, M. Uchimaya, Epik: a software program for PK a prediction and protonation state generation for drug-like molecules, *J. Comput.-Aided Mol. Des.* 21 (2007) 681–691, <https://doi.org/10.1007/s10822-007-9133-z>.
- [43] K. Roos, C. Wu, W. Damm, M. Reboul, J.M. Stevenson, C. Lu, M.K. Dahlgren, S. Mondal, W. Chen, L. Wang, R. Abel, R.A. Friesner, E.D. Harder, OPLS3e: extending force field coverage for drug-like small molecules, *J. Chem. Theory Comput.* 15 (2019) 1863–1874, <https://doi.org/10.1021/acs.jctc.8b01026>.
- [44] Biova Discovery Studio Modeling Environment, Dassault Systeme Reslease, San Diego, 2020.
- [45] B. Manasa, S. Manandhar, H. Gangadhar, K. Priya, H.B. Kumar, K.S.R. Pai, Virtual structure-based docking, WaterMap, and molecular dynamics guided identification of the potential natural compounds as inhibitors of protein-tyrosine phosphatase 1B, *J. Mol. Struct.* 1226B (2021), 129396, <https://doi.org/10.1016/j.molstruc.2020.129396>.
- [46] E. Harder, W. Damm, J. Maple, C. Wu, M.Y. Xiang, L. Wang, L. Wang, D. Lupyan, M.K. Dahlgren, J.L. Knight, J.W. Kaus, D.S. Cerutti, G. Krilov, W.L. Jorgensen, R. Abel, R.A. Friesner, OPLS3: a force field providing broad coverage of drug-like small molecules and proteins, *J. Chem. Theory Comput.* 12 (2016) 281–296, <https://doi.org/10.1021/acs.jctc.5b00864>.
- [47] Desmond Molecular Dynamics System, D. E. Shaw Research, New York, NY, 2021. Maestro-Desmond Interoperability Tools, Schrödinger, New York, NY, 2023.
- [48] M.J. Frisch, G.W. Trucks, H.B. Schlegel, G.E. Scuseria, M.A. Robb, J.R. Cheeseman, et al., Gaussian 16, Revision C.01, Gaussian, Inc, Wallingford CT, 2016.
- [49] P.J. Stephens, F.J. Devlin, C.F. Chabalowski, M.J. Frisch, Ab initio calculation of vibrational absorption and circular dichroism spectra using density functional force fields, *J. Phys. Chem.* 98 (1994) 11623–11627, <https://doi.org/10.1021/j100096a001>.
- [50] W. Willker, D. Leibfritz, R. Kerssebaum, W. Bernel, Gradient selection in inverse heteronuclear correlation spectroscopy, *Magn. Reson. Chem.* 31 (1993) 287–292, <https://doi.org/10.1002/mrc.1260310315>.
- [51] M.S. Blois, Antioxidant determinations by the use of a stable free radical, *Nature* 181 (1958) 1199, <https://doi.org/10.1038/1811199a0-00>.
- [52] X.Y. Meng, H.X. Zhang, M. Mezei, M. Cui, Molecular docking: a powerful approach for structure-based drug discovery, *Curr. Comput. Aided Drug Des.* 7 (2011) 146–157, <https://doi.org/10.2174/157340911795677602>.